31 Ambipolar diffusion in low-mass star formation. I. General comparison with the ideal MHD case

J. Masson1, G. Chabrier1,2, P. Hennebelle3, N. Vaytet2, and B. Commer¸con2

In this paper, we provide a more accurate description of the evolution of the magnetic flux redistribution during prestellar core collapse by including resistive terms in the magnetohydrodynamics (MHD) equations. We focus more particularly on the impact of ambipolar diffusion. We use the adaptive mesh refinement code RAMSES to carry out such calculations. The resistivities required to calculate the ambipolar diffusion terms were computed using a reduced chemical network of charged, neutral and grain species. The inclusion of ambipolar diffusion leads to the formation of a magnetic diffusion barrier in the vicinity of the core, preventing accumulation of magnetic flux in and around the core and amplification of the field above 0.1G. The mass and radius of the first Larson core remain similar between ideal and non-ideal MHD models. This diffusion plateau has crucial consequences on magnetic braking processes, allowing the formation of disk structures. Magnetically supported outflows launched in ideal MHD models are weakened when using non-ideal MHD. Contrary to ideal MHD misalignment between the initial rotation axis and the magnetic field direction does not significantly affect the results for a given μ, showing that the physical dissipation truly dominate over numerical diffusion. We demonstrate severe limits of the ideal MHD formalism, which yield unphysical behaviours in the long-term evolution of the system. This includes counter rotation inside the outflow, interchange instabilities, and flux redistribution triggered by numerical diffusion, none observed in non-ideal MHD. Disks with Keplerian velocity profiles form in all our non-ideal MHD simulations, with final mass and size which depend on the initial magnetisation. This ranges from a few 0.01 $M_\odot$ and 20–30 AU for the most magnetised case ($\mu = 2$) to 0.2 $M_\odot$ and 40–80 AU for a lower magnetisation ($\mu = 5$).

C:¥Users¥tomisaka¥Dropbox¥Document¥paper¥starformation newsletter¥SFN¥SFN274¥31.pdf

理想 MHD VS 非理想 MHD=Ambipolar diffusion+ Ohmic Dissipation

$$\frac{\partial \mathbf{B}}{\partial t} = \boldsymbol{\nabla} \times \left[\mathbf{v_n} \times \mathbf{B} \right.$$

オーム散逸

$$-\eta_\Omega (\boldsymbol{\nabla} \times \mathbf{B})$$

ホール効果

$$-\eta_H \left\{ (\boldsymbol{\nabla} \times \mathbf{B}) \times \frac{\mathbf{B}}{\|\mathbf{B}\|} \right\}$$

Ambipolar diffusion

$$\left. -\eta_{AD} \frac{\mathbf{B}}{\|\mathbf{B}\|} \times \left\{ (\boldsymbol{\nabla} \times \mathbf{B}) \times \frac{\mathbf{B}}{\|\mathbf{B}\|} \right\} \right],$$

$$\frac{P}{\rho} = c_s^2 \sqrt{1 + \left(\frac{n_H}{10^{-13}\,\mathrm{g\,cm^{-3}}} \right)^{\frac{4}{3}}},$$

状態方程式は

$$\mu(r) = \frac{\frac{\int_0^r dM}{\int_0^r d\phi_B}}{\left(\frac{M}{\phi} \right)_{\mathrm{crit}}}, \quad \left(\frac{M}{\phi} \right)_{\mathrm{crit}} = \frac{0.53}{3\pi} \left(\frac{5}{G} \right)^{0.5}$$
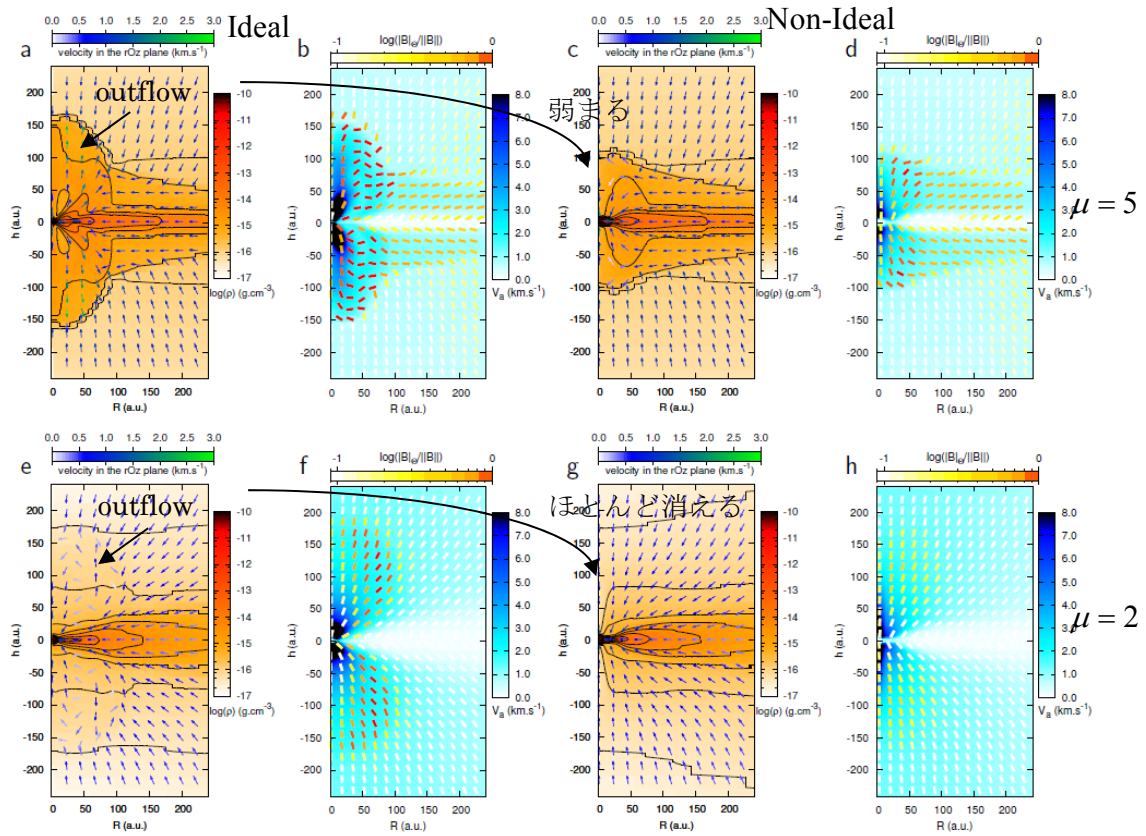
Fig. 5. Top row: $\mu = 5$, aligned case, snapshots at a time $t = 1.02\ t_{\text{free-fall}}$ (500 years after first core formation). Panel (a) shows a map of the density in the ideal MHD simulation. The black solid lines are logarithmically spaced density contours. The arrows represent the velocity field where blue to green corresponds to the increasing magnitude of the velocity in the (r, z) plane. Panel (b) is a map of the Alfvén speed (blue), with the magnetic field direction in the (r, z) plane indicated by the segments. Yellow to red in these segments corresponds to increasing relative magnitude of the toroidal component of the field compared to the total field. Panels (c) and (d) are the same as (a) and (b), respectively, but for the niMHD case. Bottom row: same as the top row for $\mu = 2$, and at the same time $t = 1.01\ t_{\text{free-fall}}$ (500 years after first core formation). Every quantity is azimuthally averaged.

アウトフロー内部で逆回転が見える、磁気タワー、交換不安定など理想 MHD だけで現れる現象ではないか。

ケプラー円盤、磁場の強い場合 $\mu = 2$ 、$M \sim 10^{-2} M_{\odot}$ で $r \sim 20 - 30\,\text{AU}$

磁場の弱い場合 $\mu = 5$ 、$M \sim 2 \times 10^{-1} M_{\odot}$ で $r \sim 40 - 80\,\text{AU}$

B//Ω（aligned）そうじゃない（misaligned）の差が顕著だったのも理想 MHD でだけ。

32 The AU Mic Debris Disk: far-infrared and submillimeter resolved imaging
Brenda C. Matthews+

We present far-infrared and submillimeter maps from the Herschel Space Observatory and the James Clerk Maxwell Telescope of the debris disk host star AU Microscopii. Disk emission is detected at 70, 160, 250, 350, 450, 500 and 850 μm. The disk is resolved at 70, 160 and 450 μm. In addition to the planetesimal belt, we detect thermal emission from AU Mic's halo for the first time. In contrast to the scattered light images, no asymmetries are evident in the disk. The fractional luminosity of the disk is 3.9×10^{-4} and its mm-grain dust mass is 0.01 $M_{\oplus}$ ($\pm 20\%$). We create a simple spatial model that reconciles the disk SED as a blackbody of 53 ± 2 K (a composite of 39 and 50 K components) and the presence of small (non-blackbody) grains which populate the extended halo. The best fit model is consistent with the "birth ring" model explored in earlier works, i.e., an edge-on dust belt extending from 8.8–40 AU, but with an additional halo component with an $r^{-1.5}$ surface density profile extending to the limits of sensitivity (140 AU). We confirm that AU Mic does not exert enough radiation force to blow out grains. For stellar mass loss rates of 10–100 $\times$ solar, compact (zero porosity) grains can only be removed if they are very small, consistently with previous work, if the porosity is 0.9, then grains approaching 0.1 μm can be removed via corpuscular forces (i.e., the stellar wind).

C:¥Users¥tomisaka¥Dropbox¥Document¥paper¥starformation newsletter¥SFN¥SFN274¥32.pdf

Herschel、JCMT,ALMA データで AU Mic
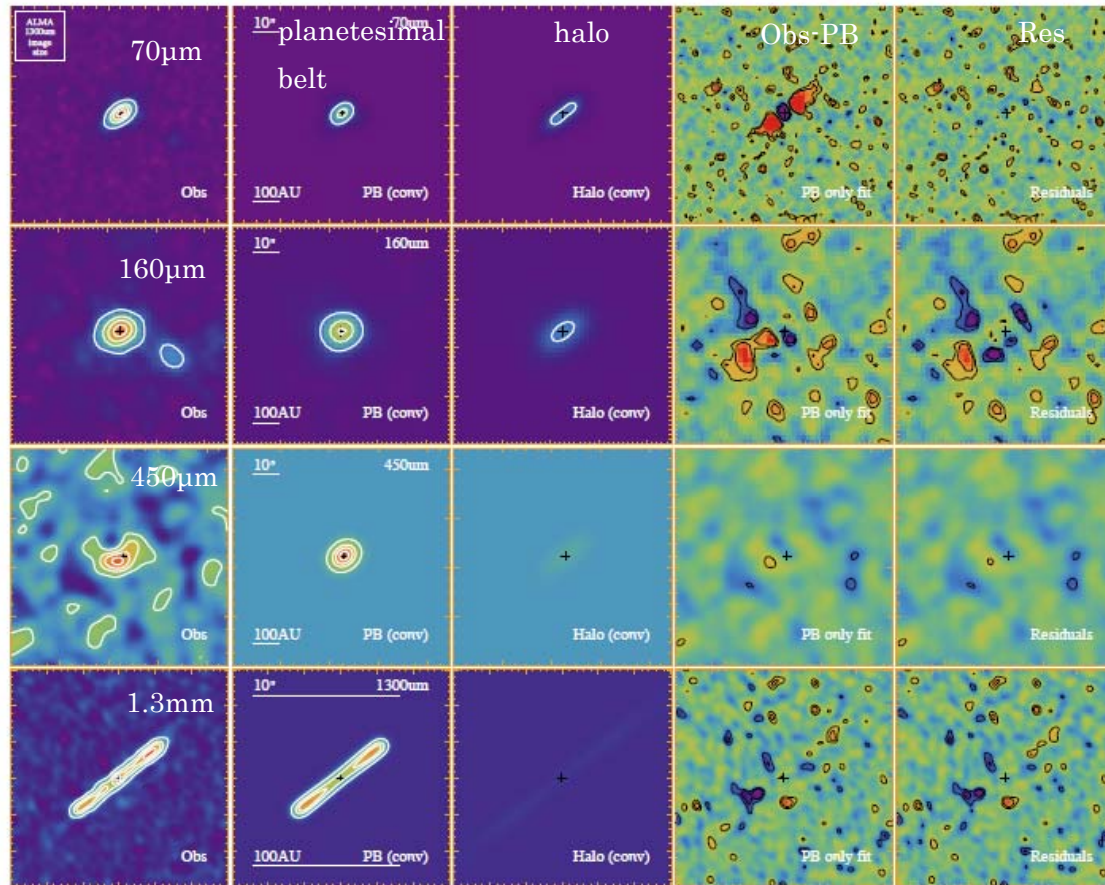
デブリディスク天体＝ディスク（planetesimal belt）＋ハローで分離できる。

PB: $\Sigma \propto r^{2.8} (8.8\,\mathrm{AU} \sim 40\,\mathrm{AU})$

温度分布 $T_{PB} = T_{0,\mathrm{PB}} r^{-1/2}$

Halo: $\Sigma \propto r^{-1.5} (40\,\mathrm{AU} \sim 140\,\mathrm{AU})$、

emissivity $(\lambda_0 / \lambda)^{\beta_\lambda} B_\lambda(T)$

温度分布 $T_{halo} = T_{0,halo} r^{-1/3}$

33. A distance limited sample of massive star forming cores from the RMS survey

L.T. Maud1,2, S.L. Lumsden1, T.J.T. Moore3, J.C. Mottram2, J.S. Urquhart4, and A. Cicchini1,5

We analyse $C^{18}O$ ($J=3$–2) data from a sample of 99 infrared-bright massive young stellar objects (MYSOs) and compact HII regions that were identified as potential molecular-outflow sources in the Red MSX source (RMS) survey. We extract a distance limited ($D < 6$ kpc) sample shown to be representative of star formation covering the transition between the source types. At the spatial resolution probed, Larson-like relationships are found for these cores, though the alternative explanation, that Larson's relations arise where surface-density-limited samples are considered, is also consistent with our data. There are no significant differences found between source properties for the MYSOs and HII regions, suggesting that the core properties are established prior to the formation of massive stars, which subsequently have little impact at the later evolutionary stages investigated. There is a strong correlation between dust-continuum and $C^{18}O$-gas masses, supporting the interpretation that both trace the same material in these IR-bright sources. A clear linear relationship is seen between the independently established core masses and luminosities. The position of MYSOs and compact HII regions in the mass-luminosity plane is consistent with the luminosity expected a cluster of protostars when using a $\sim$40% star-formation efficiency and indicates that they are at a similar evolutionary stage, near the end of the accretion phase.

C:¥Users¥tomisaka¥Dropbox¥Document¥paper¥starformation newsletter¥SFN¥SFN274¥33.pdf

MSX で赤いカラーを持つ

Massive YSO および Compact HII region に対して、D<6kpc, L<3000Lsol のサンプルに

ついて、JCMT で C18O(J=3-2)観測を行い、コアの性質を調べた。
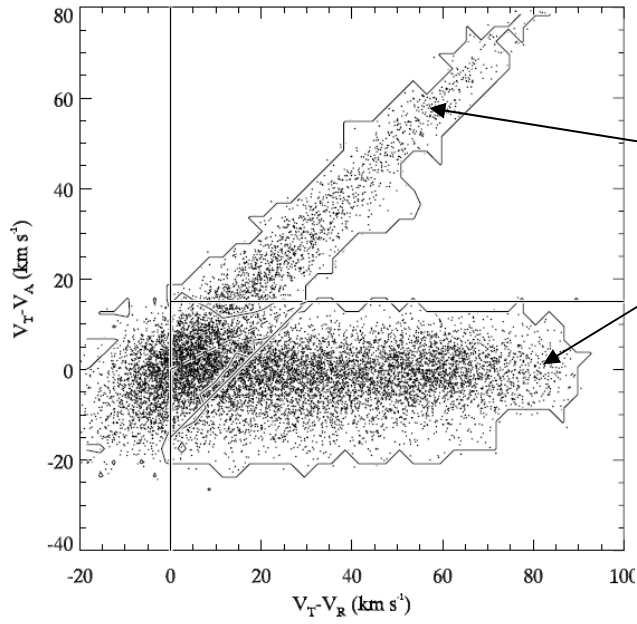

Kinematic Distance

near

far

FIG. 2.—Velocity differences for the simulated H II region complexes
The vertical axis represents the difference between the tangent-point veloc
ity and the maximum velocity at which we measured absorption, $V_t - V_a$
The horizontal axis represents the difference between the tangent-poin
velocity and the recombination-line velocity, $V_t - V_r$. The irregularl
shaped contours enclose regions where locally at least 90% of the simulate
H II regions are at the near (*top right contour*) or far (*bottom right contou*
kinematic distance. The straight solid lines mark approximations to thes
contours. Above the dashed line, at least 50% of the simulated H II region
are at the near kinematic distance, while below the dashed line, at least 50%
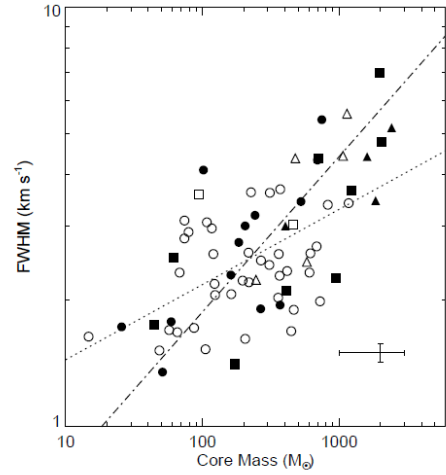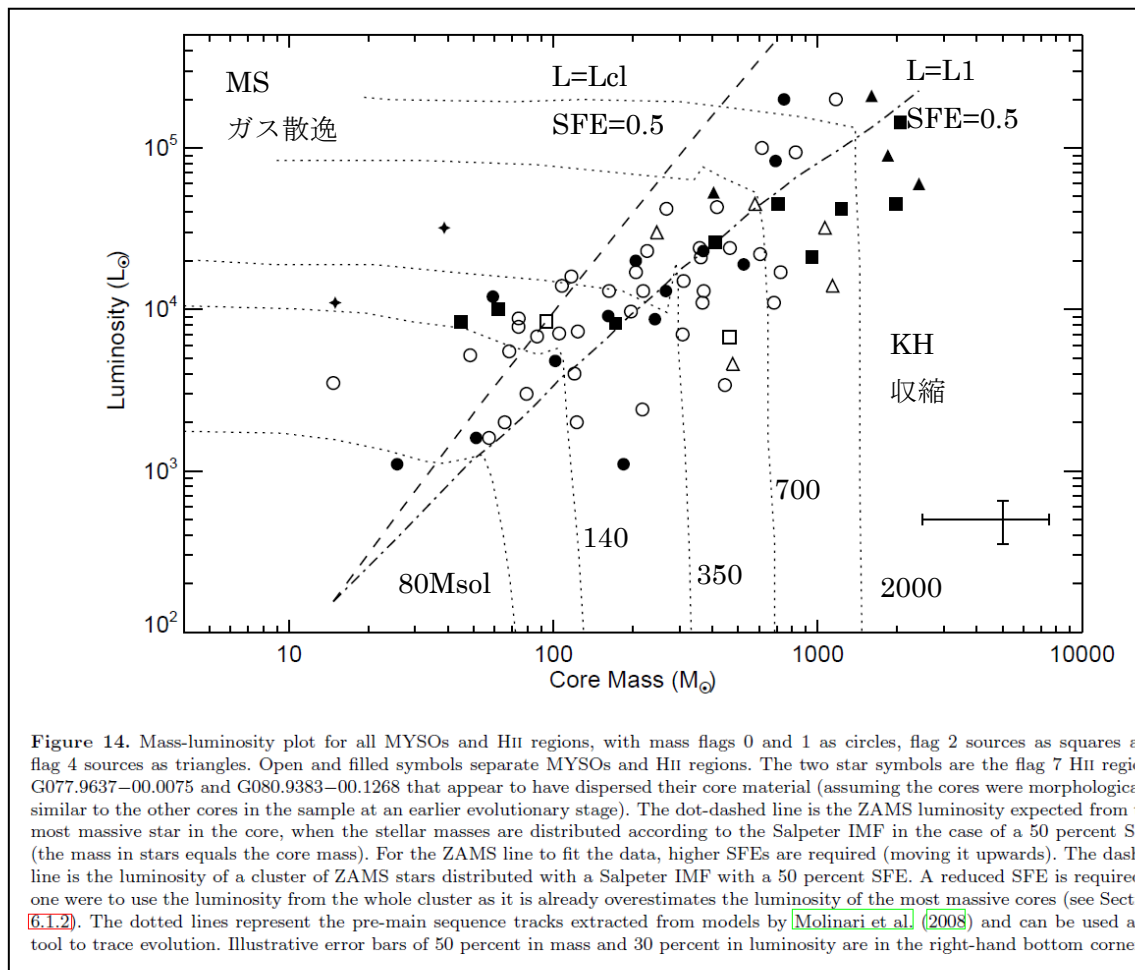are at the far kinematic distance.

Figure 10. Core mass versus the FWHM linewidth for MYSOs
and HII regions (open and filled symbols respectively). Flag 0
and 1, 2 and 4 are represented by circles, squares and triangles.
The plotted dotted line is the OLS best fit with a similar slope
(FWHM $\propto m^{0.18\pm0.04}$) to the by-eye fit from Larson (1981). The
bisector fit better represents the data given the scatter and has
a steeper slope, $FWHM \propto m^{0.37\pm0.25}$. The average uncertainty
of 5 percent in FWHM and representative 50 percent uncertainty
for the mass is shown to the bottom right.

Larson 則
HII と MYSO 同じ分布

Figure 14. Mass-luminosity plot for all MYSOs and H II regions, with mass flags 0 and 1 as circles, flag 2 sources as squares and flag 4 sources as triangles. Open and filled symbols separate MYSOs and H II regions. The two star symbols are the flag 7 H II regions G077.9637−00.0075 and G080.9383−00.1268 that appear to have dispersed their core material (assuming the cores were morphologically similar to the other cores in the sample at an earlier evolutionary stage). The dot-dashed line is the ZAMS luminosity expected from the most massive star in the core, when the stellar masses are distributed according to the Salpeter IMF in the case of a 50 percent SFE (the mass in stars equals the core mass). For the ZAMS line to fit the data, higher SFEs are required (moving it upwards). The dashed line is the luminosity of a cluster of ZAMS stars distributed with a Salpeter IMF with a 50 percent SFE. A reduced SFE is required one were to use the luminosity from the whole cluster as it is already overestimates the luminosity of the most massive cores (see Section 6.1.2). The dotted lines represent the pre-main sequence tracks extracted from models by Molinari et al. (2008) and can be used as tool to trace evolution. Illustrative error bars of 50 percent in mass and 30 percent in luminosity are in the right-hand bottom corner.

質量光度関係

34. CSO and CARMA Observations of L1157. I. A Deep Search for Hydroxylamine (NH2OH)
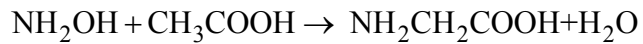
Brett A. McGuire1,2 +

A deep search for the potential glycine precursor hydroxylamine (NH_2OH) using the Caltech Submillimeter Observatory (CSO) at $\lambda=1.3$ mm and the Combined Array for Research in Millimeter-wave Astronomy (CARMA) at $\lambda=3$ mm is presented toward the molecular outflow L1157, targeting the B1 and B2 shocked regions. We report non-detections of NH_2OH in both sources. We a perform non-LTE analysis of CH_3OH observed in our CSO spectra to derive kinetic temperatures and densities in the shocked regions. Using these parameters, we derive upper limit column densities of NH_2OH of $\leq 1.4 \times 10^{13}$ cm^{-2} and $\leq 1.5 \times 10^{13}$ cm^{-2} toward the B1 and B2 shocks, respectively, and upper limit relative abundances of $N_{NH_2OH}/N_{H_2} \leq 1.4 \times 10^{-8}$ and $\leq 1.5 \times 10^{-8}$, respectively.

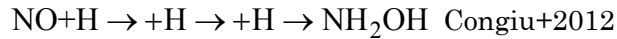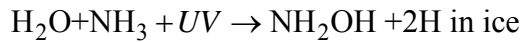C:\Users\tomisaka\Dropbox\Document\paper\starformation newsletter\SFN\SFN274\34.pdf
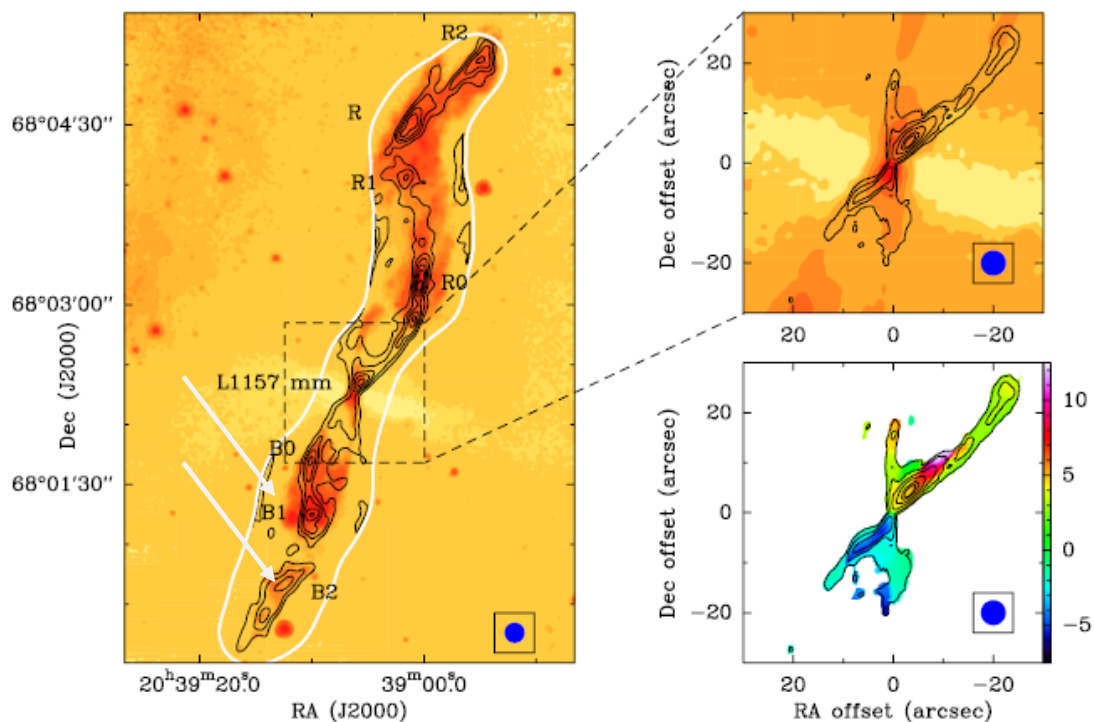
アミノ酸の捜索

ヒドロキシルアミンはアミノ酸グリシンの前駆体

$$NH_2OH + CH_3COOH \rightarrow NH_2CH_2COOH + H_2O$$

ヒドロキシルアミン＋酢酸＝グリシン

ヒドロキシルアミンの生成パス

$$H_2O + NH_3 + UV \rightarrow NH_2OH + 2H \text{ in ice}$$

$$NO + H \rightarrow +H \rightarrow +H \rightarrow NH_2OH \quad Congiu+2012$$

$$NH_3 + O \rightarrow NH_2OH \text{ in ice} \quad He+2015$$

ダストマントルで低温で生成され急に多くが気相に出てくる場所として衝撃波領域を探す。

H2 に対するアバンダンスは、 $NH_2OH/H_2 \sim 10^{-6}(cond), 10^{-7}(gas)$ が想定されるが、

得られた H2 に対するアバンダンスは、 $NH_2OH/H_2 < 1.4 \times 10^{-8}(B1), 1.5 \times 10^{-8}(B2)$

Woojin Kwon+ (2015)astro-ph/1510.2155

35. High resolution Brγ spectro-interferometry of the transitional Herbig Ae/Be star HD 100546: a Keplerian gaseous disc inside the inner rim

I. Mendigut´ıa1, W.J. de Wit2, R.D. Oudmaijer1, J.R. Fairlamb1, A.D. Carciofi3, J.D. Ilee4 and R.G.Vieira3

We present spatially and spectrally resolved Brγ emission around the planet-hosting, transitional Herbig Ae/Be star HD 100546. Aiming to gain insight into the physical origin of the line in possible relation to accretion processes, we carried out Brγ spectro-interferometry using AMBER/VLTI from three different baselines achieving spatial and spectral resolutions of $2 - 4$ mas and 12000. The Brγ visibility is larger than that of the continuum for all baselines. Differential phases reveal a shift between the photocentre of the Brγ line –displaced ~ 0.6 mas (0.06 au at 100 pc) NE from the star– and that of the K-band continuum emission –displaced ~ 0.3 mas NE from the star. The photocentres of the redshifted and blueshifted components of the Brγ line are located NW and SE from the photocentre of the peak line emission, respectively. Moreover, the photocentre of the fastest velocity bins within the spectral line tends to be closer to that of the peak emission than the photocentre of the slowest velocity bins. Our results are consistent with a Brγ emitting region inside the dust inner rim ($\lesssim 0.25$ au) and extending very close to the central star, with a Keplerian, disc-like structure rotating counter-clockwise, and most probably flared ($\sim 25\circ$). Even though the main contribution to the Brγ line does not come from gas magnetically channelled on to the star, accretion on to HD 100546 could be magnetospheric, implying a mass accretion rate of a few 10^{-7} M$_\odot$ yr^{-1}. This value indicates that the observed gas has to be replenished on time-scales of a few months to years, perhaps by planet-induced flows from the outer to the inner disc as has been reported for similar systems.

C:¥Users¥tomisaka¥Dropbox¥Document¥paper¥starformation newsletter¥SFN¥SFN274¥35.pdf
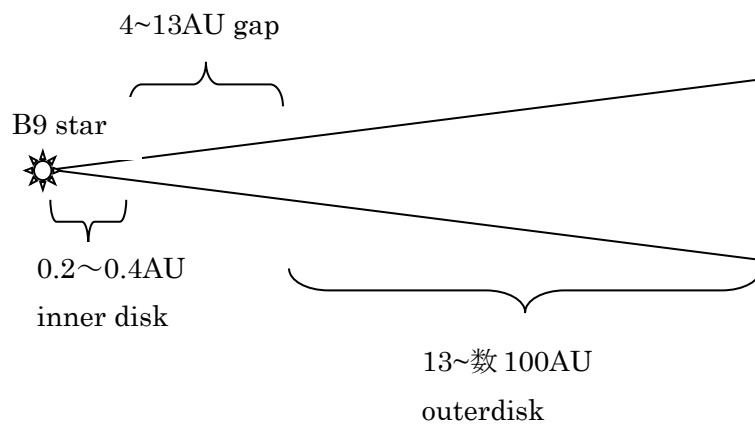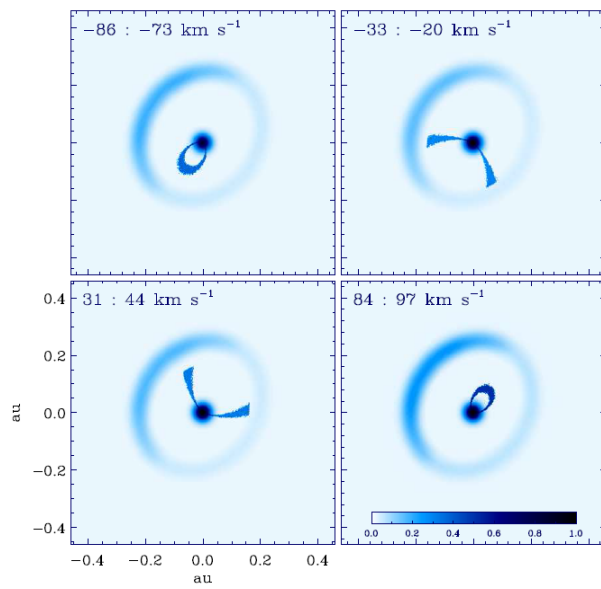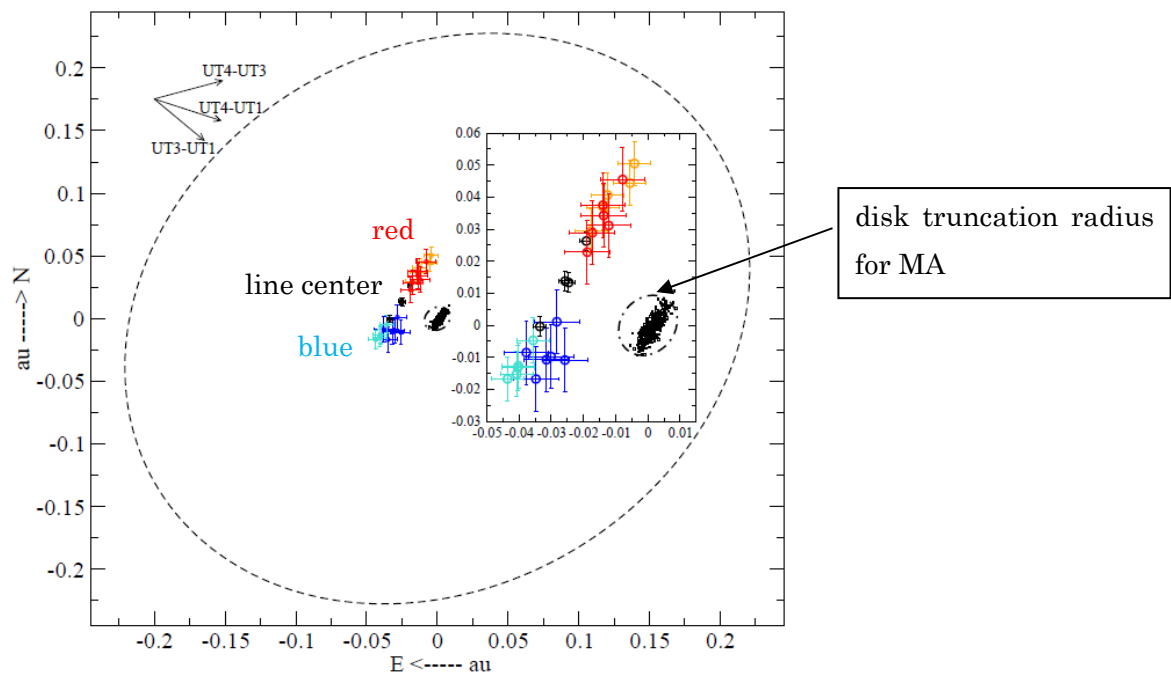
Br γ 干渉観測

HD 100546 transitional Ae/Be

多数派、Br γ 輝線は、内側ディスク連続波よりコンパクト

少数派、Br γ 輝線は、より広がっている。

Classical T-Tauri stars 磁気圏を通って降着(Magnetospheric accretion)。

HAeBe 円盤から星へ境界層(Boundary layer)を通して直接降着(BL)

4~13AU gap

B9 star

0.2〜0.4AU
inner disk

13~数100AU
outerdisk

Brγ 輝線は内側ダストへりの内側に分布、ディスク形状か